Electronic Supplementary Material (ESI) for CrystEngComm.

Supporting Information

Thermosalience coupled to abrupt spin crossover with dynamic ligand motion in an iron(II) molecular crystal

Hiroaki Hagiwara* and Souta Konomura

Department of Chemistry, Faculty of Education, Gifu University, Yanagido 1-1, Gifu 501-1193, Japan

*E-mail: hagiwara@gifu-u.ac.jp

Table of Contents

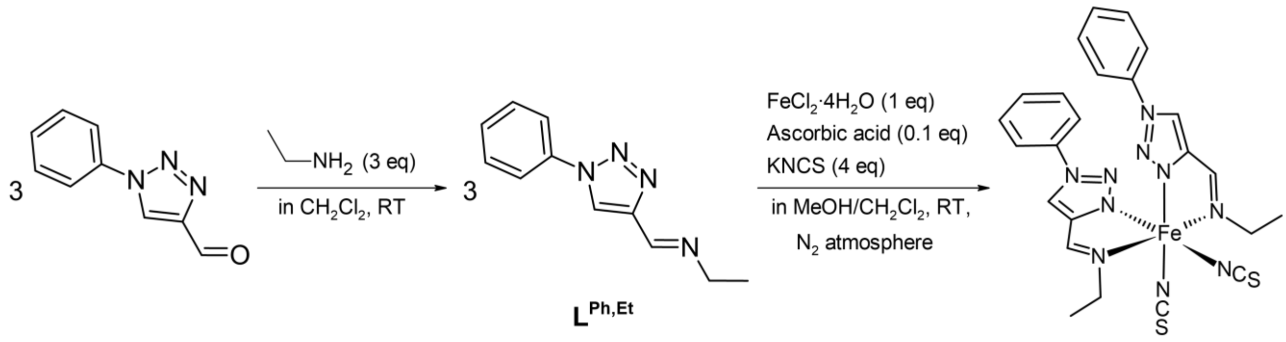

Scheme S1 Preparation of $[Fe(L^{Ph,Et})_2(NCS)_2]$ (**1**).

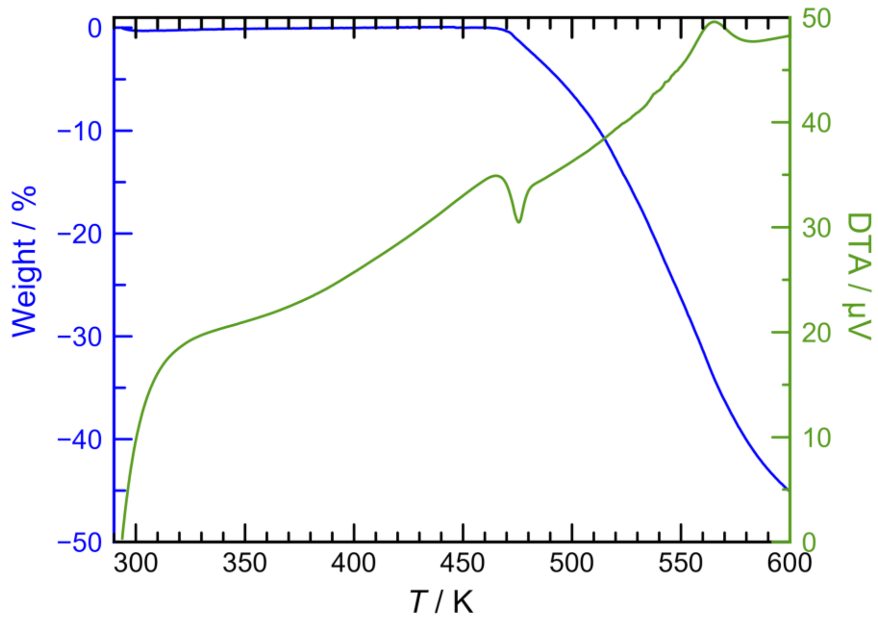

Fig. S1 TG/DTA curve of **1** at a sweep rate of 10 K min^{-1}.

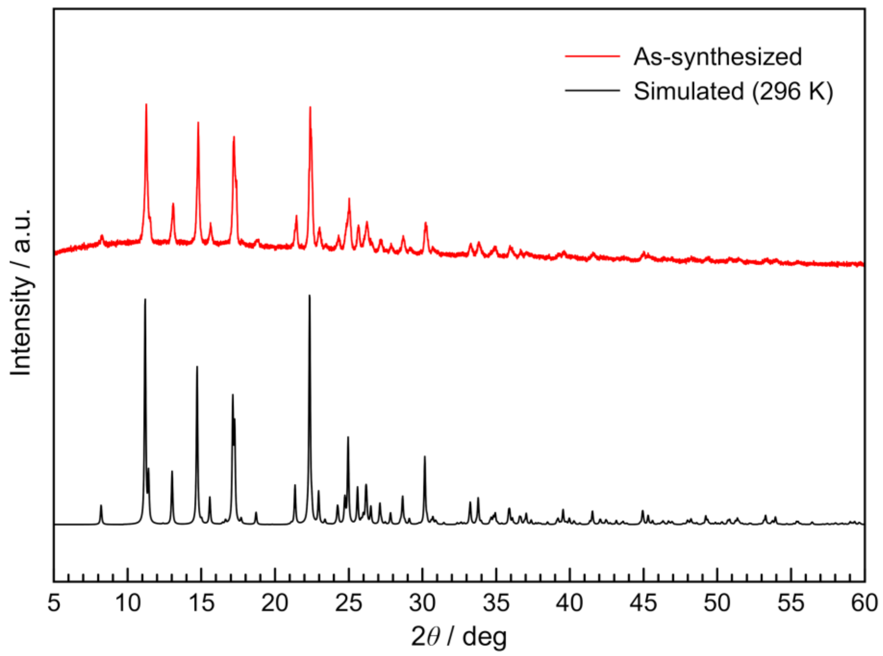

Fig. S2 Experimental PXRD pattern of **1** (red) at room temperature (RT) with the one calculated from the single crystal X-ray diffraction data (gray).

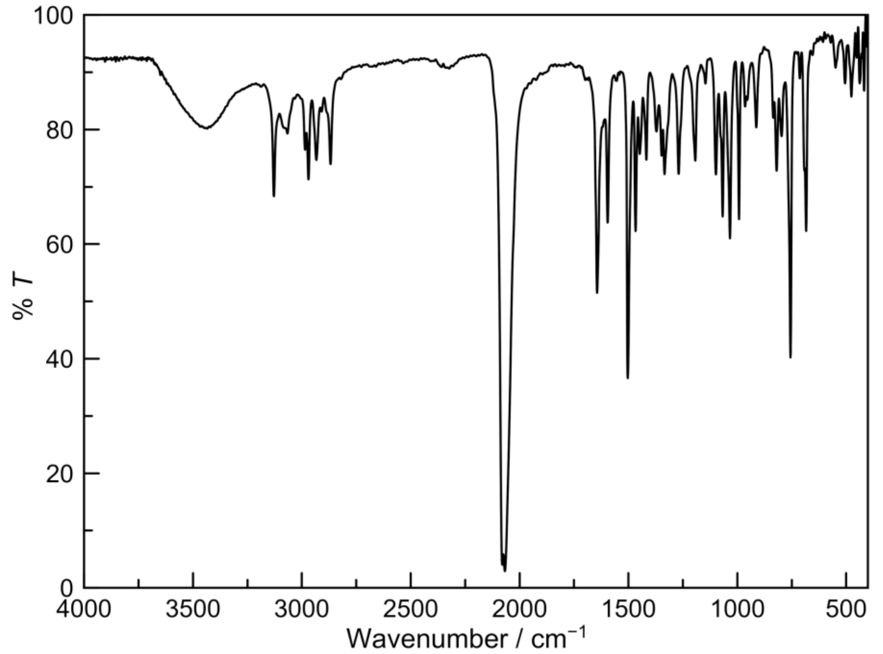

Fig. S3 IR spectrum (KBr) for **1** at RT.

Table S1 X–ray Crystallographic Data for **1**

Complex	$[Fe(L^{Ph,Et})_2(NCS)_2]$ (**1**)					
Temperature	100 K	140 K	170 K	190 K	230 K	296 K
Formula	$C_{24}H_{24}FeN_{10}S_2$					
Formula weight	572.50					
Crystal system	Monoclinic					
Space group	$P2_1/c$	$P2_1/c$	$P2_1/c$	$C2/c$	$C2/c$	$C2/c$
a, Å	11.1742(7)	11.2176(6)	11.2148(6)	10.7263(3)	10.7423(3)	10.8131(4)
b, Å	11.4148(5)	11.4699(4)	11.4800(4)	11.7000(4)	11.7166(4)	11.8013(5)
c, Å	20.2335(12)	20.3726(9)	20.4163(10)	21.7531(7)	21.8606(8)	21.8679(7)
β, deg	98.288(6)	98.280(4)	98.314(5)	99.441(3)	99.702(3)	99.875(3)
V, Å^3	2553.9(3)	2593.9(2)	2600.9(2)	2692.99(15)	2712.09(16)	2749.19(18)
Z	4	4	4	4	4	4
T, K	100(2)	140(2)	170(2)	190(2)	230(2)	296(2)
μ (Mo Kα), mm^{-1}	0.790	0.777	0.775	0.749	0.743	0.733
d_{calcd}, g cm^{-3}	1.489	1.466	1.462	1.412	1.402	1.383
Reflections collected	20932	21332	21494	11647	11752	11936
Independent reflections	7210	7277	7332	3834	3863	3793
R_{int}	0.0385	0.0309	0.0353	0.0142	0.0144	0.0159
R_1[a] (I>2sigma(I))	0.0574	0.0572	0.0654	0.0370	0.0353	0.0381
R_1[a] (all data)	0.0899	0.0936	0.1142	0.0452	0.0452	0.0536
wR_2[b] (I>2sigma(I))	0.1200	0.1125	0.1408	0.0990	0.0962	0.1043
wR_2[b] (all data)	0.1332	0.1260	0.1610	0.1050	0.1034	0.1141
S	1.098	1.100	1.074	1.062	1.056	1.039
CCDC number	2131324	2131325	2131326	2131327	2131328	2131329

[a] $R_1 = \Sigma||Fo|-|Fc||/\Sigma|Fo|$.

[b] $wR_2 = [\Sigma w(|Fo|^2-|Fc|^2)^2/\Sigma w(|Fo|^2)^2]^{1/2}$.

Table S2 Relevant coordination bond lengths and angles for **1**

Temperature	100 K	140 K	170 K	190 K	230 K	296 K
Bond Lengths (Å)						
Fe–N3$_{triazole}$	1.931(2)	1.939(2)	1.942(3)	2.1972(13)	2.2244(13)	2.2386(14)
Fe–N4$_{imine}$	1.989(2)	2.001(2)	2.002(3)	2.1819(14)	2.2009(13)	2.2087(16)
Fe–N5$_{NCS}$	1.941(2)	1.952(2)	1.952(3)	2.0600(18)	2.0671(16)	2.0716(18)
Fe–N8$_{triazole}$	1.941(2)	1.948(2)	1.955(3)			
Fe–N9$_{imine}$	1.978(2)	1.989(2)	1.989(3)			
Fe–N10$_{NCS}$	1.935(2)	1.946(2)	1.948(3)			
Fe–N3$^{*}_{triazole}$				2.1972(13)	2.2244(13)	2.2386(14)
Fe–N4$^{*}_{imine}$				2.1819(14)	2.2009(13)	2.2087(16)
Fe–N5$^{*}_{NCS}$				2.0600(18)	2.0671(16)	2.0716(18)
Bond Angles (°)						
N3–Fe–N4	80.91(9)	80.90(9)	80.74(11)			
N3–Fe–N5	90.88(9)	90.74(9)	90.59(11)			
N3–Fe–N8	90.08(9)	90.17(9)	90.22(11)			
N3–Fe–N9	94.32(9)	94.25(9)	94.10(11)			
N3–Fe–N10	174.27(10)	174.24(9)	174.33(12)			
N5–Fe–N4	88.14(9)	88.21(9)	88.25(12)			
N5–Fe–N9	93.69(10)	93.71(9)	93.89(12)			
N8–Fe–N4	97.42(9)	97.30(9)	97.18(11)			
N8–Fe–N5	174.44(10)	174.49(10)	174.57(12)			
N8–Fe–N9	80.77(10)	80.80(9)	80.69(11)			
N9–Fe–N4	174.93(9)	174.82(9)	174.44(12)			
N10–Fe–N4	93.50(9)	93.47(9)	93.72(12)			
N10–Fe–N5	90.22(10)	90.31(10)	90.42(12)			
N10–Fe–N8	89.36(9)	89.33(9)	89.31(11)			
N10–Fe–N9	91.22(9)	91.33(9)	91.40(12)			
N3*–Fe–N3				85.70(7)	85.36(7)	85.25(7)
N4*–Fe–N3				93.58(5)	93.34(5)	93.16(5)
N4–Fe–N3				75.58(5)	74.96(5)	74.75(5)
N4–Fe–N3*				93.58(5)	93.33(5)	93.16(5)
N4*–Fe–N3*				75.58(5)	74.96(5)	74.76(5)
N4–Fe–N4*				165.39(8)	164.26(8)	163.76(9)
N5–Fe–N3*				169.87(6)	169.46(6)	169.46(7)
N5–Fe–N3				89.48(6)	89.36(6)	89.39(7)
N5*–Fe–N3				169.87(6)	169.46(6)	169.46(7)
N5*–Fe–N3*				89.48(6)	89.36(6)	89.39(7)
N5–Fe–N4				93.84(6)	94.09(6)	94.18(7)
N5–Fe–N4*				95.86(6)	96.30(6)	96.53(7)
N5*–Fe–N4*				93.84(6)	94.09(6)	94.18(7)
N5*–Fe–N4				95.86(6)	96.30(6)	96.53(7)
N5–Fe–N5*				96.60(10)	97.24(10)	97.27(11)

* Symmetry code: 1−x, Y, 1/2−z

Table S3 Selected structural parameters for **1**

Temperature	100 K	140 K	170 K	190 K	230 K	296 K
Average Fe–N, Å	1.952	1.962	1.965	2.146	2.164	2.173
Σ^{a}, °	42.22	42.01	42.57	67.34	70.70	71.46
Θ^{b}, °	144.03	142.85	143.71	187.28	194.31	196.43
$V_{Oh}{}^{c}$, Å^3	9.818	9.971	10.002	12.868	13.156	13.308
S(Oh)[d]	0.460	0.457	0.462	0.863	0.926	0.940
N2–N3–C8–C9, °	−177.2(2)	−177.2(2)	−177.2(3)	−179.2(1)	−179.3(1)	−179.3(2)
N3–C8–C9–N4, °	0.8(3)	0.7(3)	0.8(4)	−0.5(2)	−0.4(2)	−0.4(3)
C8–C9–N4–C10, °	−179.8(2)	−179.7(2)	−179.7(3)	178.8(1)	178.7(1)	178.7(2)
C9–N4–C10–C11, °	−104.9(3)	−104.3(3)	−104.2(3)	−103.0(2)	−103.0(2)	−102.3(2)
N7–N8–C20–C21, °	−178.9(2)	−178.6(2)	−178.7(3)			
N8–C20–C21–N9, °	−2.1(3)	−2.4(3)	−2.3(4)			
C20–C21–N9–C22, °	−179.4(2)	−179.7(2)	179.9(3)			
C21–N9–C22–C23, °	−8.9(4)	−9.3(4)	−10.6(5)			

[a] Σ = the sum of $|90 - \varphi|$ for the 12 *cis* N–Fe–N angles in the octahedral coordination sphere[S1] calculated using the program OctaDist.[S2]
[b] Θ = the sum of $|60 - \theta|$ for the 24 N–Fe–N angles describing the trigonal twist angles[S3] calculated using the program OctaDist.[S2]
[c] Calculated using the program OLEX2.[S4]
[d] Calculated using the program Shape 2.1.[S5]

Table S4 Intermolecular CH⋯S interactions of **1**

Temp (K)	CH⋯X	H⋯X (Å)	C⋯X (Å)	C–H⋯X (°)	Symmetry code
296	C6–H6⋯S1	2.9807	3.796(2)	147.2	1−x, 1−y, −z
	C7–H7⋯S1	2.9592	3.677(2)	135.1	1/2+X, −1/2+Y, Z
	C9–H9⋯S1	2.8969	3.670(2)	141.4	1/2+X, −1/2+Y, Z
230	C6–H6⋯S1	2.9294	3.755(2)	147.4	1−x, 1−y, −z
	C7–H7⋯S1	2.9096	3.636(2)	135.1	1/2+X, −1/2+Y, Z
	C9–H9⋯S1	2.8816	3.655(2)	140.4	1/2+X, −1/2+Y, Z
190	C6–H6⋯S1	2.9101	3.742(2)	147.0	1−x, 1−y, −z
	C7–H7⋯S1	2.8928	3.622(2)	134.4	1/2+X, −1/2+Y, Z
	C9–H9⋯S1	2.8628	3.639(2)	139.7	1/2+X, −1/2+Y, Z
170	C6–H6⋯S2	2.873	3.782(4)	160.5	X, 3/2−Y, −1/2+Z
	C9–H9⋯S2	2.817	3.598(4)	140.1	2−x, −1/2+Y, 3/2−z
	C21–H21⋯S1	2.747	3.581(4)	147.0	1−x, −1/2+Y, 3/2−z
140	C6–H6⋯S2	2.8651	3.779(3)	161.7	X, 3/2−Y, −1/2+Z
	C9–H9⋯S2	2.8195	3.596(3)	139.5	2−x, −1/2+Y, 3/2−z
	C21–H21⋯S1	2.7439	3.579(3)	147.1	1−x, −1/2+Y, 3/2−z
100	C6–H6⋯S2	2.8401	3.757(3)	162.4	X, 3/2−Y, −1/2+Z
	C9–H9⋯S2	2.8043	3.578(3)	139.2	2−x, −1/2+Y, 3/2−z
	C21–H21⋯S1	2.7227	3.558(3)	147.1	1−x, −1/2+Y, 3/2−z

Table S5 Definition of centroids (Cg) for chelate and aromatic rings of **1**

Temp (K)	Ring	Abbreviation	Related atoms	Symmetry code
296, 230, 190	Chelate	Cg1	Fe1–N3–C8–C9–N4	
	Chelate	Cg2	Fe1–N3*–C8*–C9*–N4*	1−x, y, 1/2−z
	Triazolyl	Cg3	N1–N2–N3–C8–C7	
	Phenyl	Cg4	C1–C2–C3–C4–C5–C6	
170, 140, 100	Chelate	Cg1	Fe1–N3–C8–C9–N4	
	Chelate	Cg2	Fe1–N8–C20–C21–N9	
	Triazolyl	Cg3	N1–N2–N3–C8–C7	
	Triazolyl	Cg4	N6–N7–N8–C20–C19	
	Phenyl	Cg5	C1–C2–C3–C4–C5–C6	
	Phenyl	Cg6	C13–C14–C15–C16–C17–C18	

Table S6 Intermolecular contacts for π···π interactions in **1**

Temp (K)	π···π	X···X (Å)	Symmetry code
296	Cg4···Cg4	3.7458(13)	1/2−X, 1/2−Y, −Z
	C2···C6	3.501(3)	1/2−X, 1/2−Y, −Z
	C6···C2	3.501(3)	1/2−X, 1/2−Y, −Z
	C4···N1	3.529(3)	1/2−X, 1/2−Y, −Z
	N1···C4	3.529(3)	1/2−X, 1/2−Y, −Z
230	Cg4···Cg4	3.7196(11)	1/2−X, 1/2−Y, −Z
	C2···C6	3.484(3)	1/2−X, 1/2−Y, −Z
	C6···C2	3.484(3)	1/2−X, 1/2−Y, −Z
	C4···N1	3.513(2)	1/2−X, 1/2−Y, −Z
	N1···C4	3.513(2)	1/2−X, 1/2−Y, −Z
190	Cg4···Cg4	3.7108(12)	1/2−X, 1/2−Y, −Z
	C2···C6	3.475(3)	1/2−X, 1/2−Y, −Z
	C6···C2	3.475(3)	1/2−X, 1/2−Y, −Z
	C4···N1	3.506(2)	1/2−X, 1/2−Y, −Z
	N1···C4	3.506(2)	1/2−X, 1/2−Y, −Z
170	Cg5···Cg5	3.772(2)	1−X, 1−Y, 1−Z
	C2···C6	3.372(5)	1−X, 1−Y, 1−Z
	C6···C2	3.372(5)	1−X, 1−Y, 1−Z
	C4···N1	3.391(4)	1−X, 1−Y, 1−Z
	N1···C4	3.391(4)	1−X, 1−Y, 1−Z
	Cg6···Cg6	3.693(2)	2−X, 1−Y, 2−Z
	C13···C15	3.375(5)	2−X, 1−Y, 2−Z
	C15···C13	3.375(5)	2−X, 1−Y, 2−Z
	C16···N6	3.545(4)	2−X, 1−Y, 2−Z
	N6···C16	3.545(4)	2−X, 1−Y, 2−Z
140	Cg5···Cg5	3.7664(15)	1−X, 1−Y, 1−Z
	C2···C6	3.361(4)	1−X, 1−Y, 1−Z
	C6···C2	3.361(4)	1−X, 1−Y, 1−Z
	C4···N1	3.380(3)	1−X, 1−Y, 1−Z
	N1···C4	3.380(3)	1−X, 1−Y, 1−Z
	Cg6···Cg6	3.6833(14)	2−X, 1−Y, 2−Z
	C13···C15	3.355(4)	2−X, 1−Y, 2−Z
	C15···C13	3.355(4)	2−X, 1−Y, 2−Z
	C16···N6	3.537(3)	2−X, 1−Y, 2−Z
	N6···C16	3.537(3)	2−X, 1−Y, 2−Z
100	Cg5···Cg5	3.7475(15)	1−X, 1−Y, 1−Z
	C2···C6	3.336(3)	1−X, 1−Y, 1−Z
	C6···C2	3.336(3)	1−X, 1−Y, 1−Z
	C4···N1	3.352(3)	1−X, 1−Y, 1−Z
	N1···C4	3.352(3)	1−X, 1−Y, 1−Z
	Cg6···Cg6	3.6621(14)	2−X, 1−Y, 2−Z
	C13···C15	3.328(4)	2−X, 1−Y, 2−Z
	C15···C13	3.328(4)	2−X, 1−Y, 2−Z
	C16···N6	3.514(3)	2−X, 1−Y, 2−Z
	N6···C16	3.514(3)	2−X, 1−Y, 2−Z

Temp, K	All	H···H	S···H/H···S	C···H/H···C
296	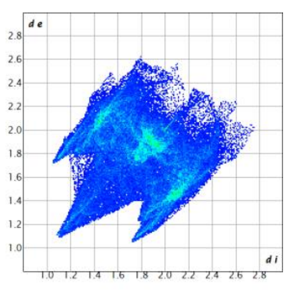	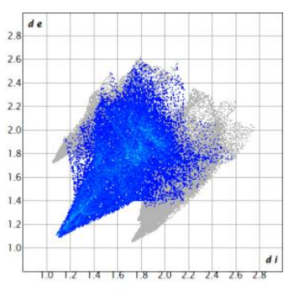	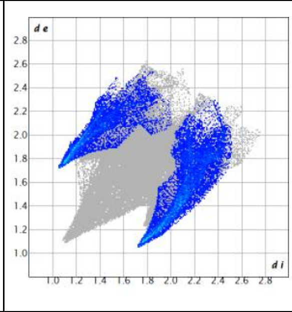	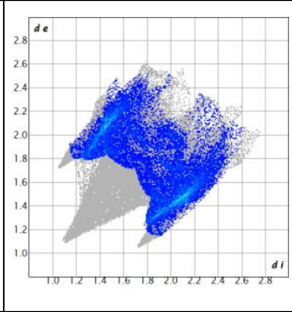
230	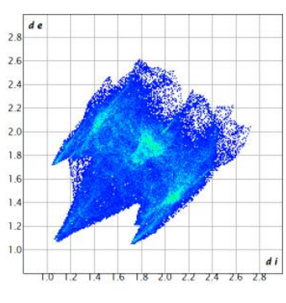	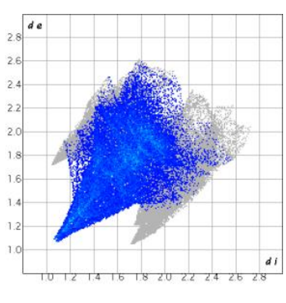	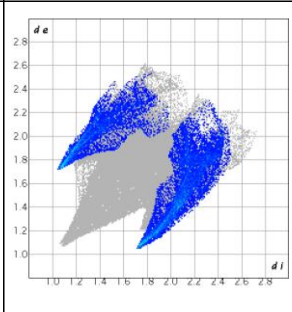	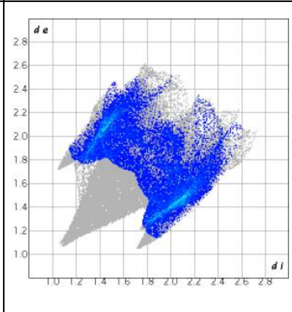
190	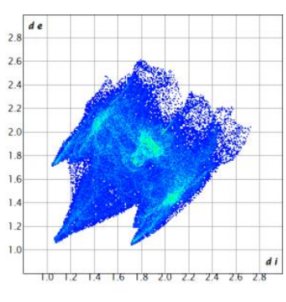	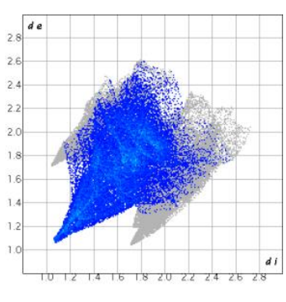	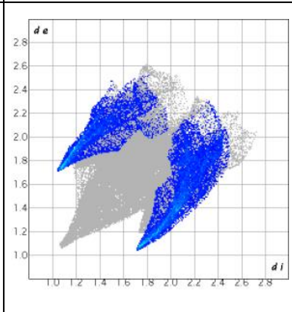	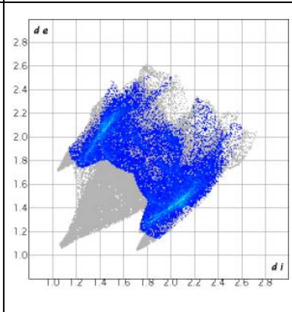
170	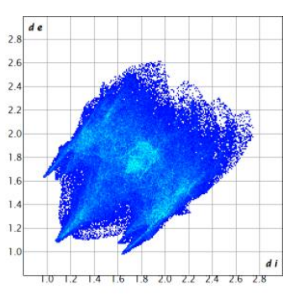	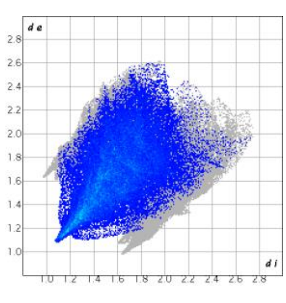	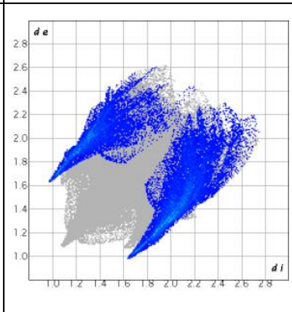	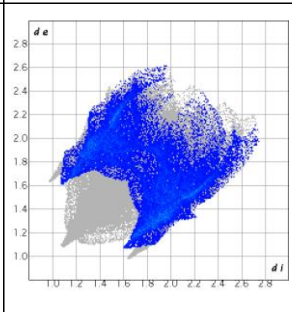
140	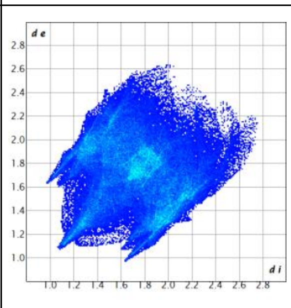	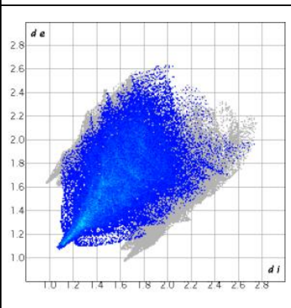	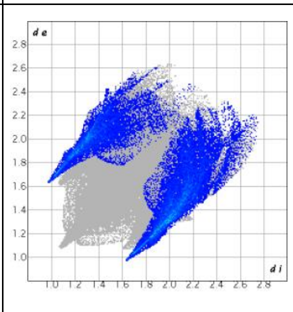	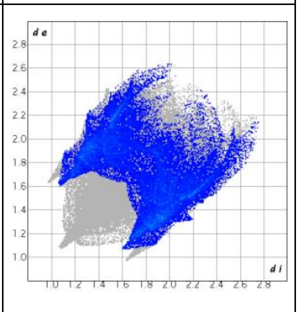
100	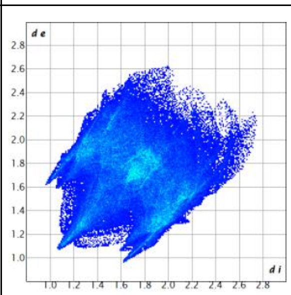	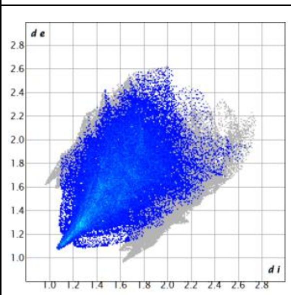	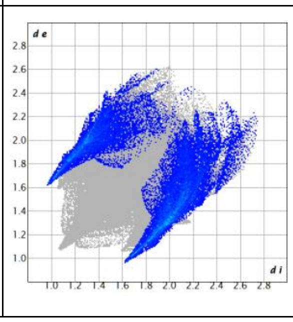	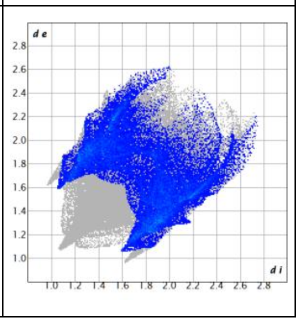

Fig. S4 Two-dimensional (2D) fingerprint plots for **1**. The d_i and d_e values are the closest internal and external distances (Å) from given points on the Hirshfeld surface.

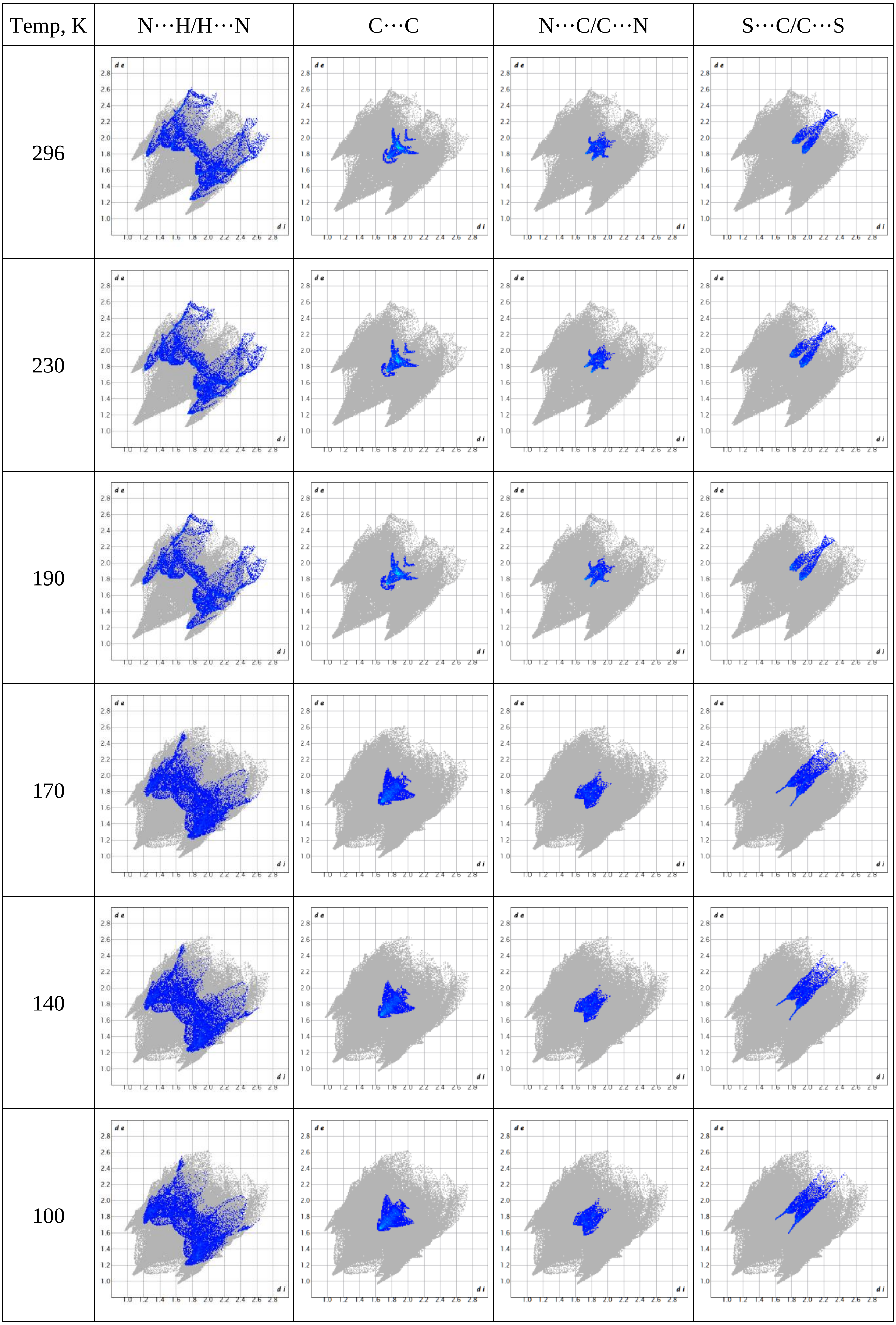

Fig. S4 2D fingerprint plots for **1** (continue). The d_i and d_e values are the closest internal and external distances (Å) from given points on the Hirshfeld surface.

Temp, K	View from ligand A	View from ligand B	Transparent view from ligand A	Transparent view from ligand B
296	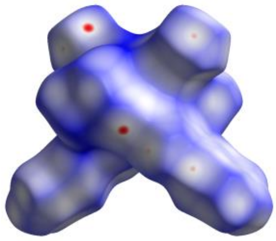		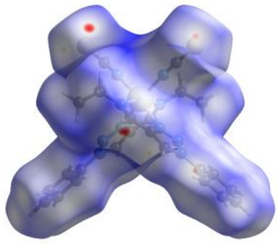	
230	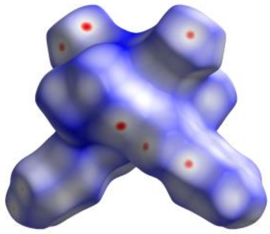		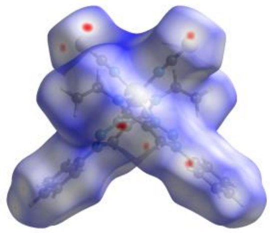	
190	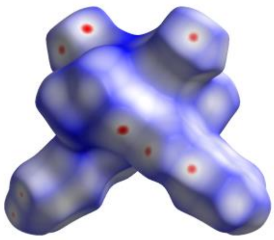		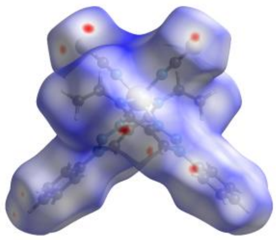	
170	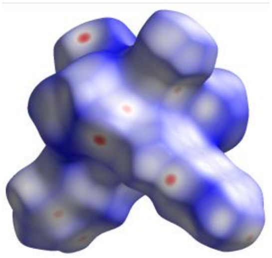	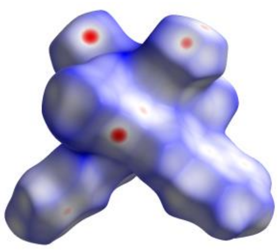	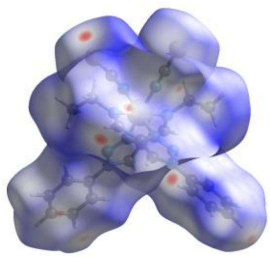	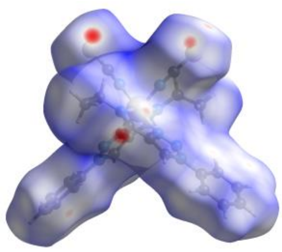
140	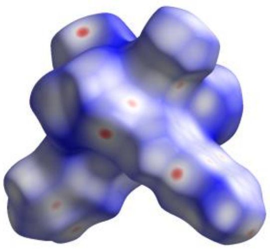	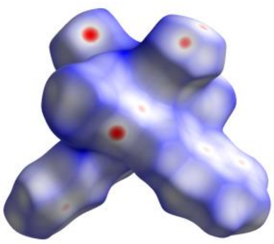	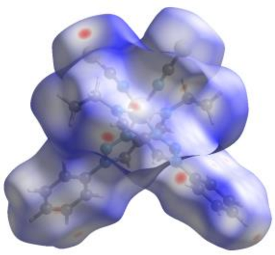	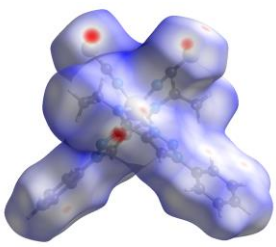
100	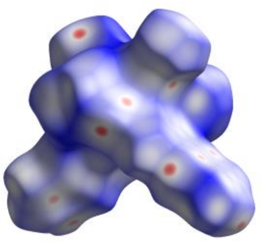	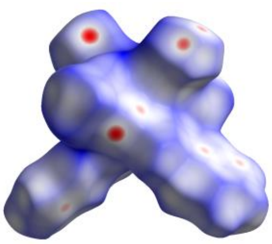	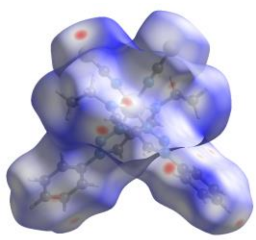	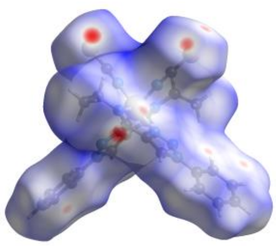

Fig. S5 Hirshfeld surfaces mapped with the normalized contact distance (d_{norm}) for **1**.

<table>
<tr><th>Temp, K</th><th>H···H
view from ligand A</th><th>H···H
view from ligand B</th><th>S···H/H···S
view from ligand A</th><th>S···H/H···S
view from ligand B</th></tr>
<tr><td>296</td><td colspan="2">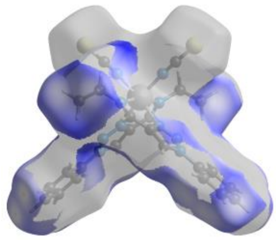</td><td colspan="2">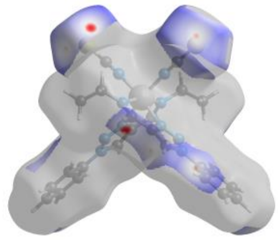</td></tr>
<tr><td>230</td><td colspan="2">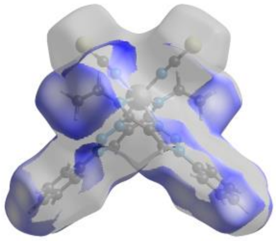</td><td colspan="2">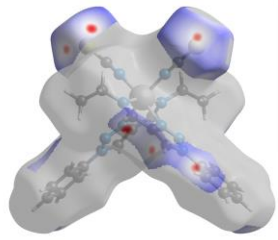</td></tr>
<tr><td>190</td><td colspan="2">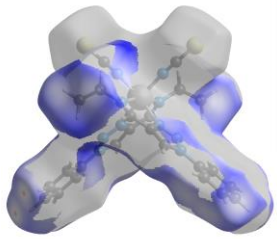</td><td colspan="2">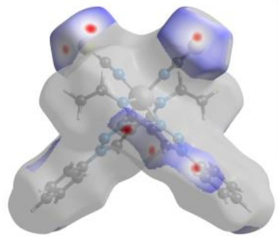</td></tr>
<tr><td>170</td><td>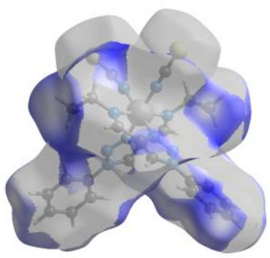</td><td>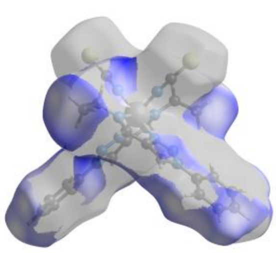</td><td>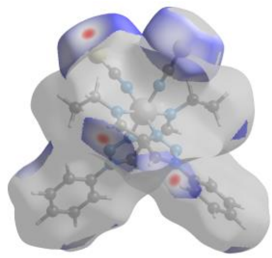</td><td>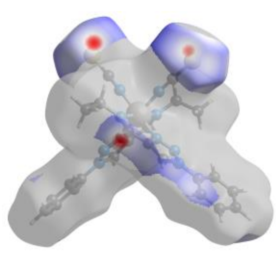</td></tr>
<tr><td>140</td><td>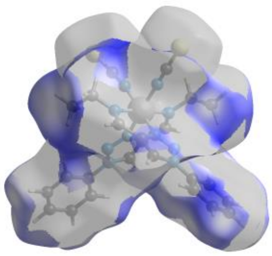</td><td>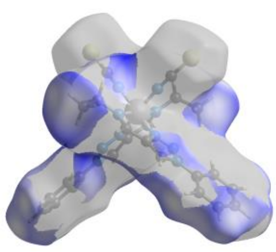</td><td>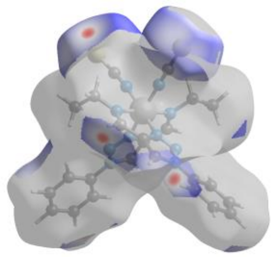</td><td>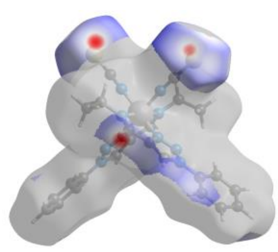</td></tr>
<tr><td>100</td><td>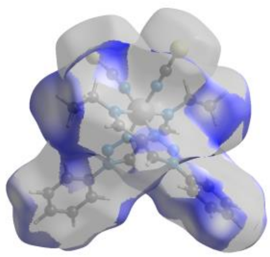</td><td>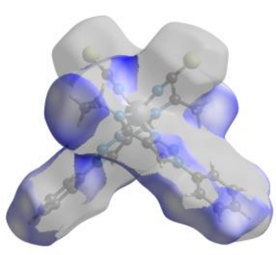</td><td>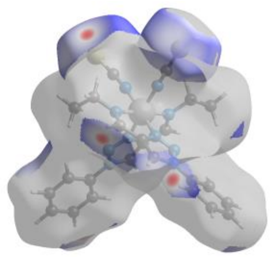</td><td>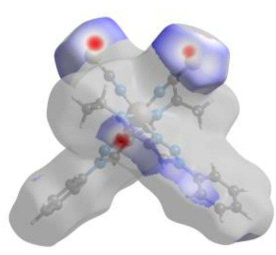</td></tr>
</table>

Fig. S6 Hirshfeld surfaces of the specific contacts with d_{norm} for **1**.

Temp, K	C···H/H···C view from ligand A	C···H/H···C view from ligand B	N···H/H···N view from ligand A	N···H/H···N view from ligand B
296	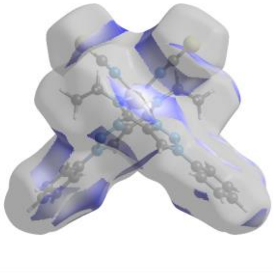		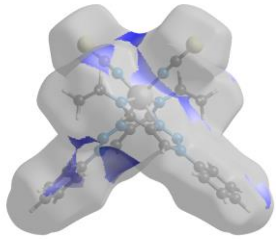	
230	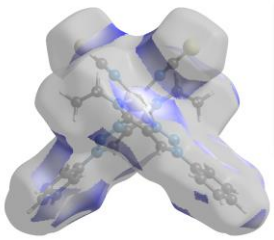		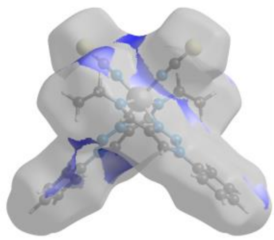	
190	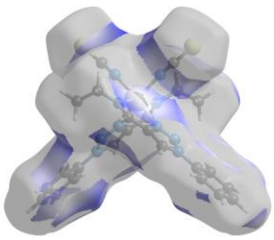		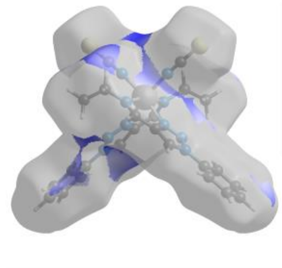	
170	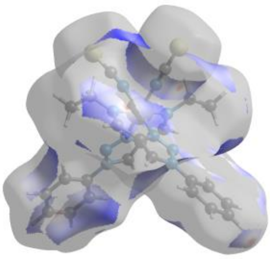	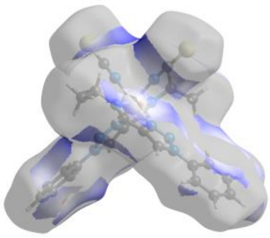	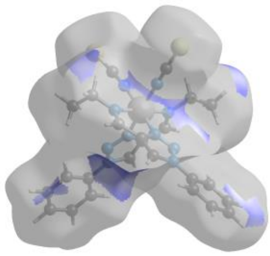	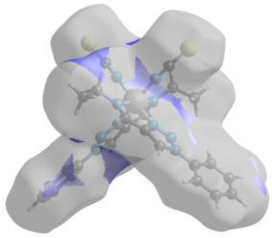
140	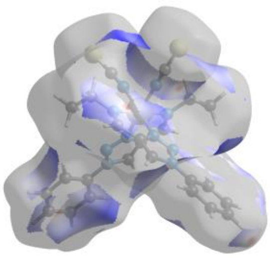	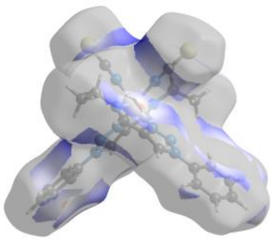	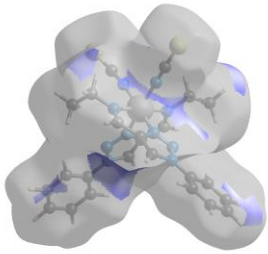	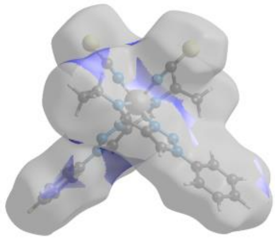
100	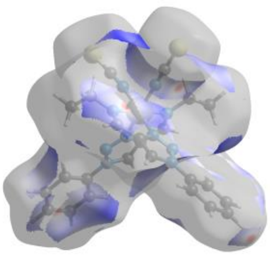	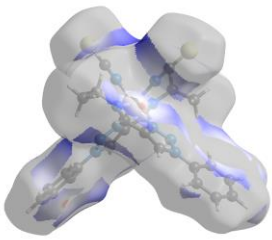	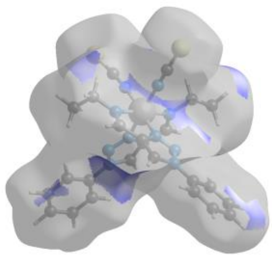	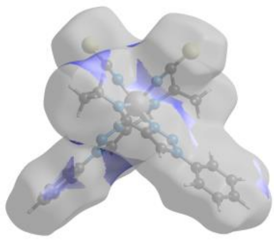

Fig. S6 Hirshfeld surfaces of the specific contacts with d_{norm} for **1** (continue).

<table>
<tr><th>Temp, K</th><th>C···C
view from ligand A</th><th>C···C
view from ligand B</th><th>N···C/C···N
view from ligand A</th><th>N···C/C···N
view from ligand B</th></tr>
<tr><td>296</td><td colspan="2">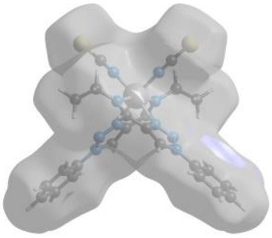</td><td colspan="2">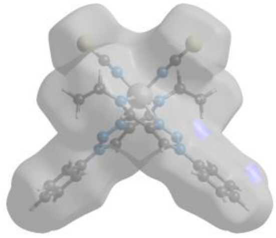</td></tr>
<tr><td>230</td><td colspan="2">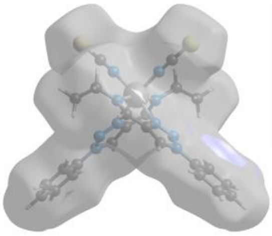</td><td colspan="2">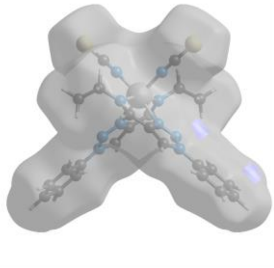</td></tr>
<tr><td>190</td><td colspan="2">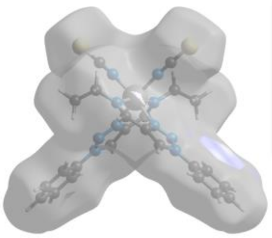</td><td colspan="2">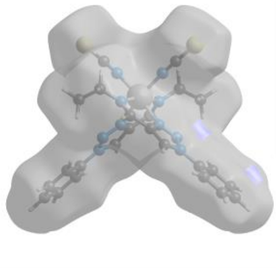</td></tr>
<tr><td>170</td><td>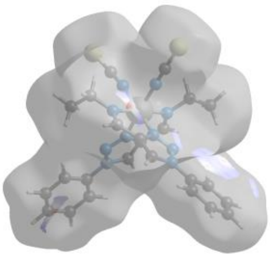</td><td>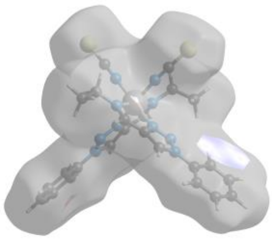</td><td>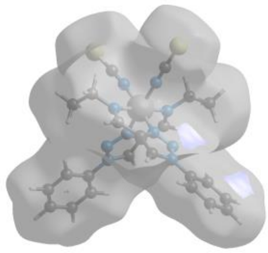</td><td>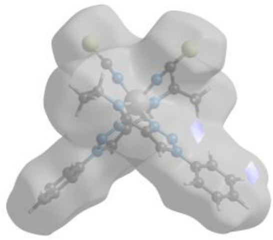</td></tr>
<tr><td>140</td><td>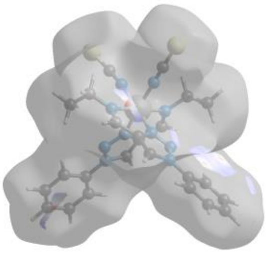</td><td>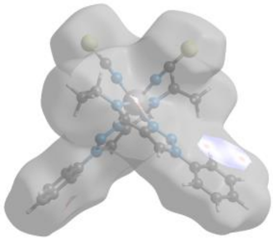</td><td>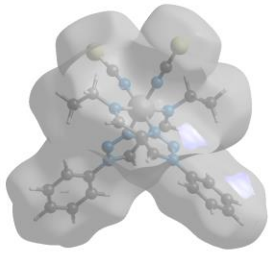</td><td>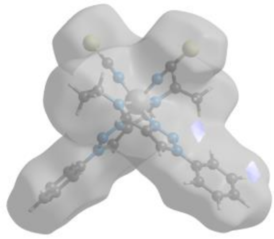</td></tr>
<tr><td>100</td><td>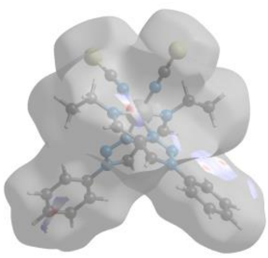</td><td>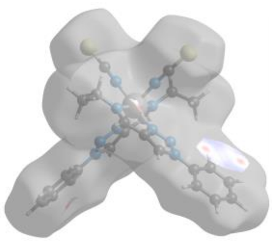</td><td>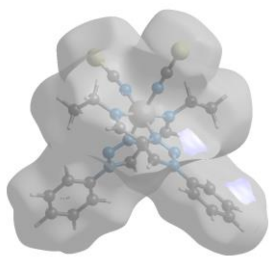</td><td>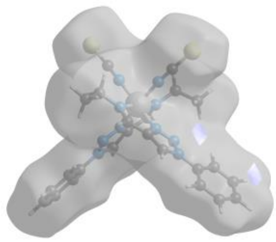</td></tr>
</table>

Fig. S6 Hirshfeld surfaces of the specific contacts with d_{norm} for **1** (continue).

<table>
<tr><th>Temp, K</th><th>S···C/C···S
view from ligand A</th><th>S···C/C···S
view from ligand B</th></tr>
<tr><td>296</td><td colspan="2">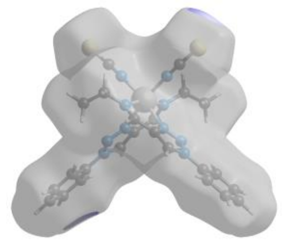</td></tr>
<tr><td>230</td><td colspan="2">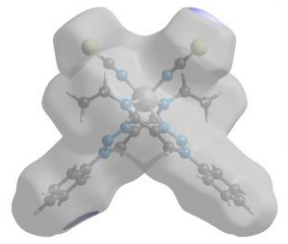</td></tr>
<tr><td>190</td><td colspan="2">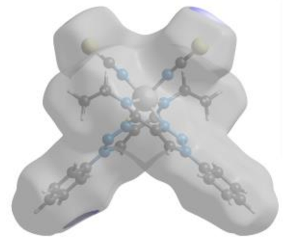</td></tr>
<tr><td>170</td><td>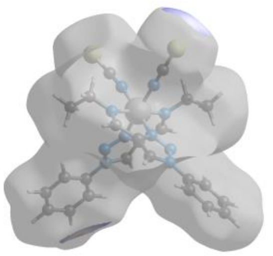</td><td>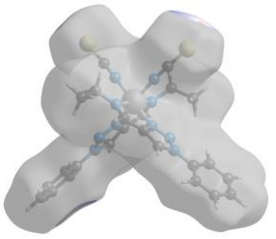</td></tr>
<tr><td>140</td><td>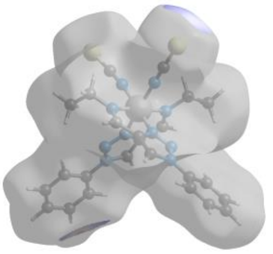</td><td>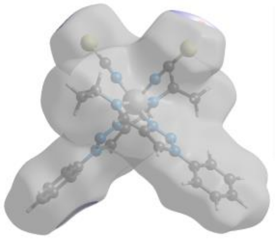</td></tr>
<tr><td>100</td><td>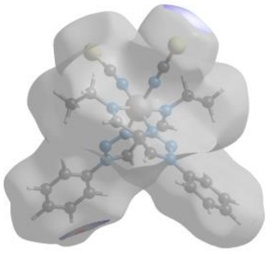</td><td>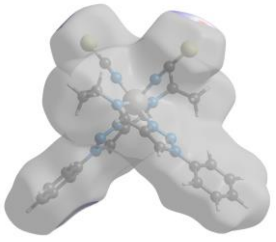</td></tr>
</table>

Fig. S6 Hirshfeld surfaces of the specific contacts with d_{norm} for **1** (continue).

Table S7 Relative percentage contributions of interatomic contacts to the Hirshfeld surface for **1**

X···X	100 K	140 K	170 K	190 K	230 K	296 K
H···H	37.9	37.9	37.9	37.0	37.0	37.1
S···H/ H···S	20.4	20.5	20.6	20.0	20.1	20.4
C···H/H···C	24.6	24.6	24.5	25.0	25.0	24.9
N···H/H···N	8.8	8.8	8.8	9.8	9.8	9.6
C···C	3.5	3.5	3.4	3.4	3.4	3.3
N···C/C···N	2.1	2.0	2.0	2.0	2.0	2.0
S···C/C···S	2.5	2.5	2.5	2.3	2.3	2.2
S···S	0.2	0.2	0.2	0.5	0.5	0.5
All	100	100	100	100	100	100

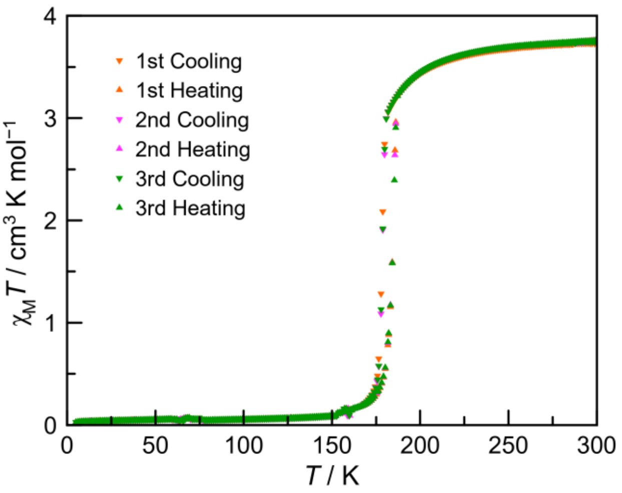

Fig. S7 Temperature dependence of the $\chi_M T$ product over three consecutive thermal cycles for **1** at a sweep rate of 1 K min^{-1}.

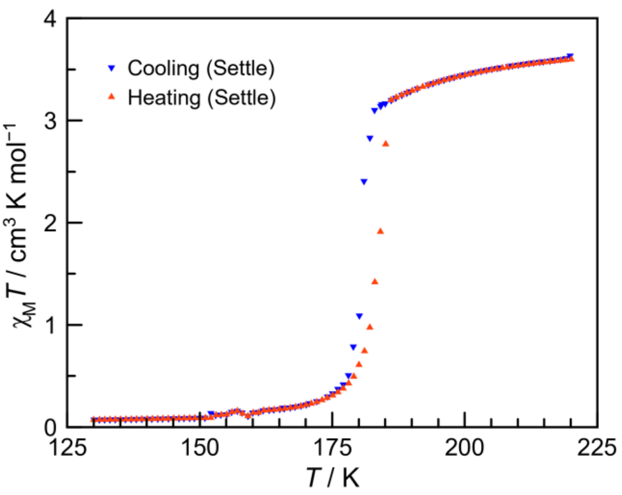

Fig. S8 $\chi_M T$ vs T plots of **1** collected in the settle mode in the cooling (inverted triangles) and heating (triangles) modes.

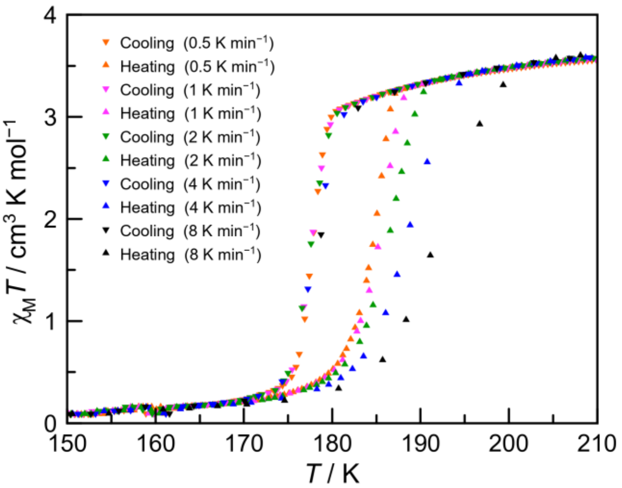

Fig. S9 $\chi_M T$ vs T plots of **1** collected in the cooling (inverted triangles) and heating (triangles) modes at various sweep rates of 0.5, 1, 2, 4, and 8 K min^{-1}.

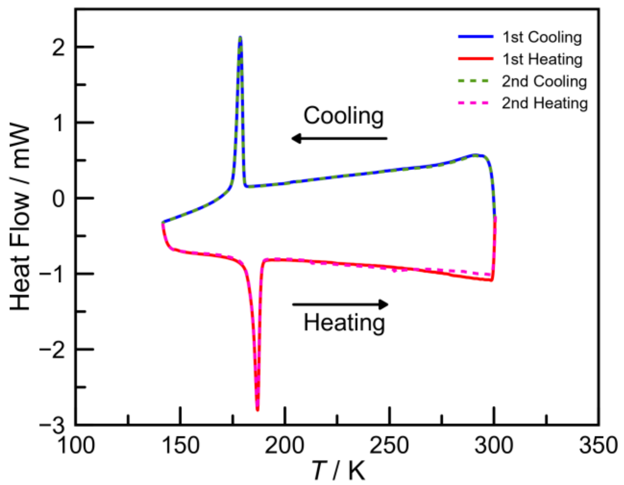

Fig. S10 DSC curves over two consecutive thermal cycles of **1** at a sweep rate of 5 K min^{-1}.

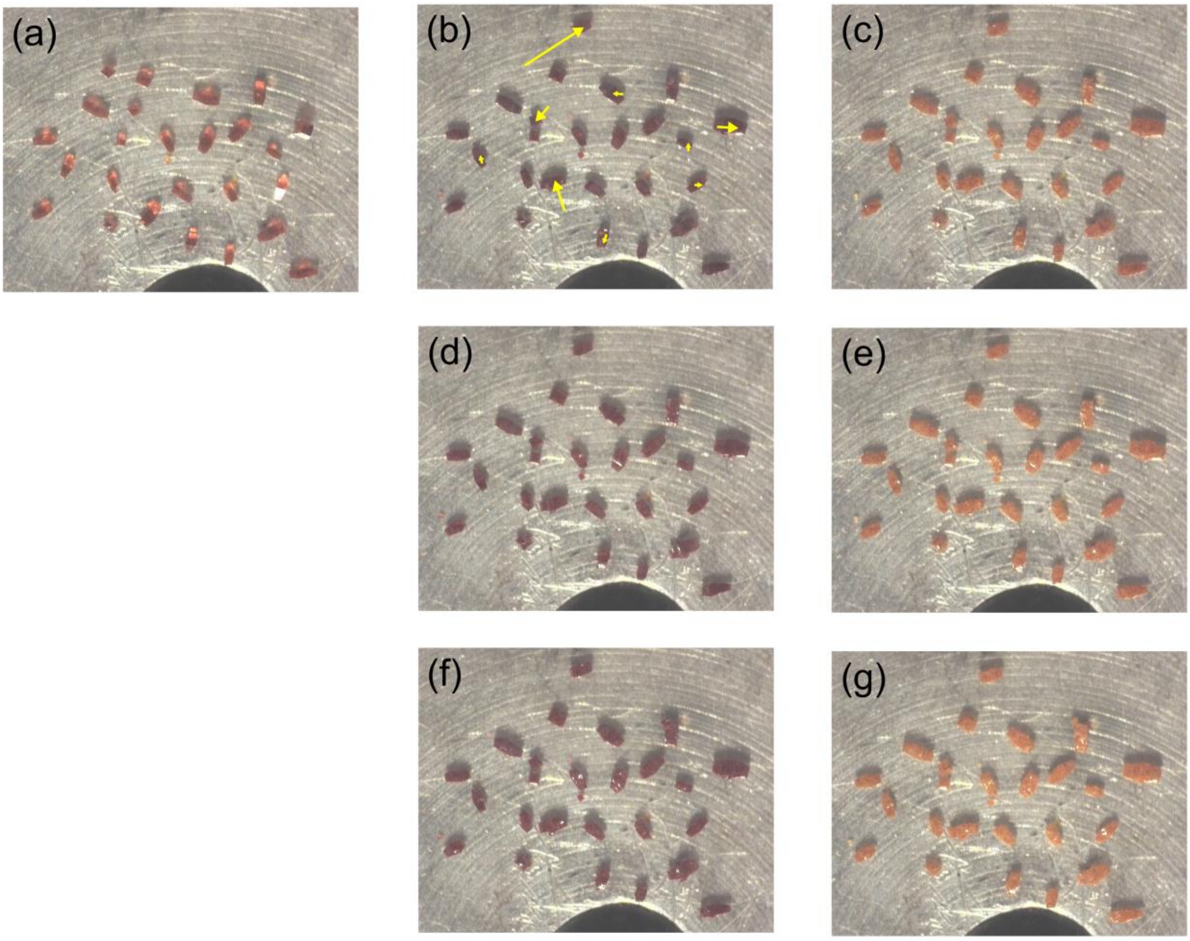

Fig. S11 Cold-stage microscopy images of single crystals of **1** over three consecutive thermal cycles between 20 °C to –180 °C at a scan rate of 75 °C min^{-1}. (a) Pristine crystals at 20 °C. (b) Crystals showing thermosalience and concomitant color change after first cooling. (c) Crystals after first heating. (d) Crystals after second cooling. (e) Crystals after second heating. (f) Crystals after third cooling. (g) Crystals after third heating. In the heating−cooling cycles from (b) to (g), the temperature variations induce volume change, cracks, and thermochromism of the crystals with no TS events.

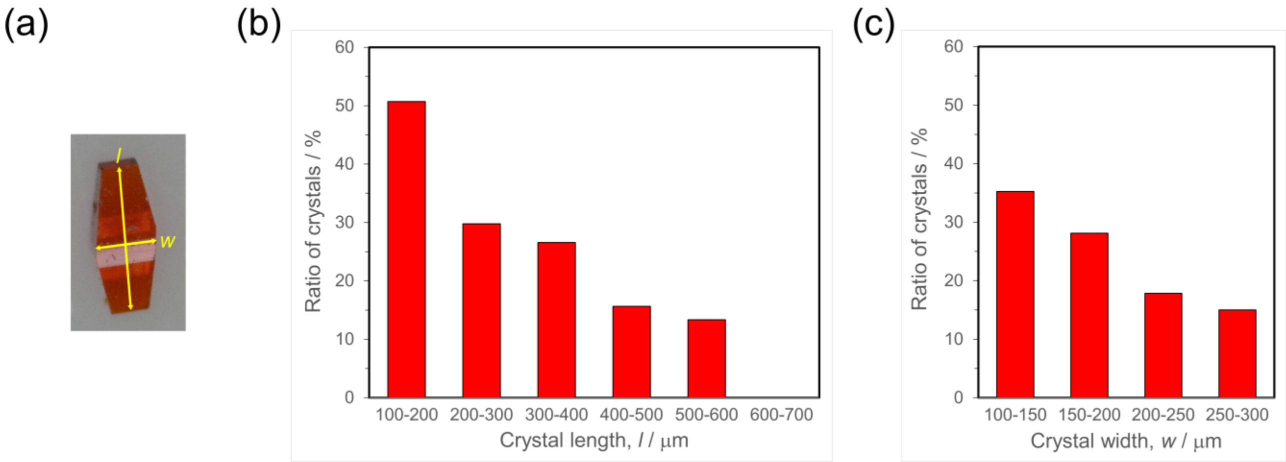

Fig. S12 Definition of crystal size of length, *l* and width, *w* (a), and distribution of the relative ratio of the observed TS effects for single crystals of **1** in *l* (b) and *w* (c). The relative ratio was calculated for the number of crystals in particular size range showing TS effects by dividing it by the total number of crystals in the same range.

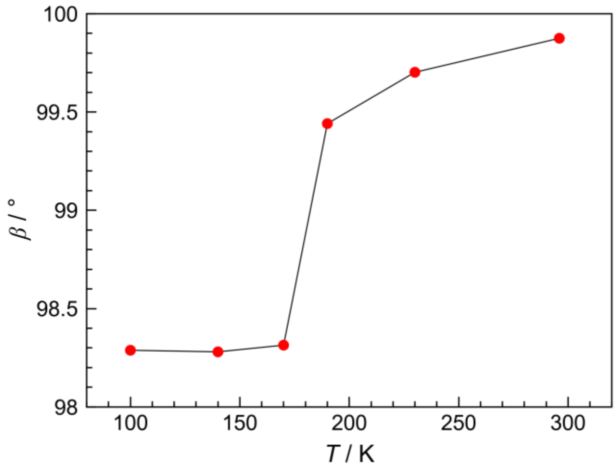

Fig. S13 Temperature dependence of the β angle for **1**.

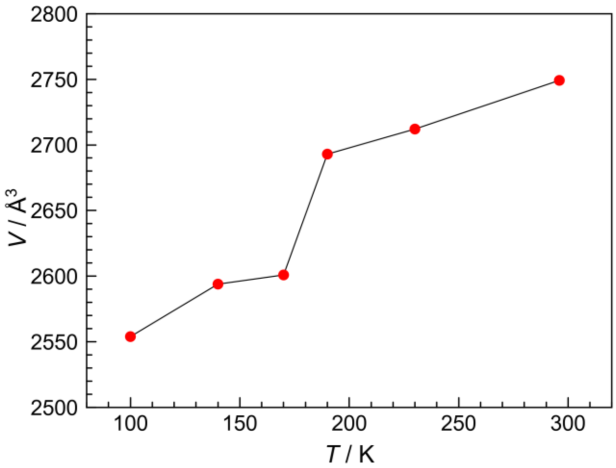

Fig. S14 Temperature dependence of V for **1**.

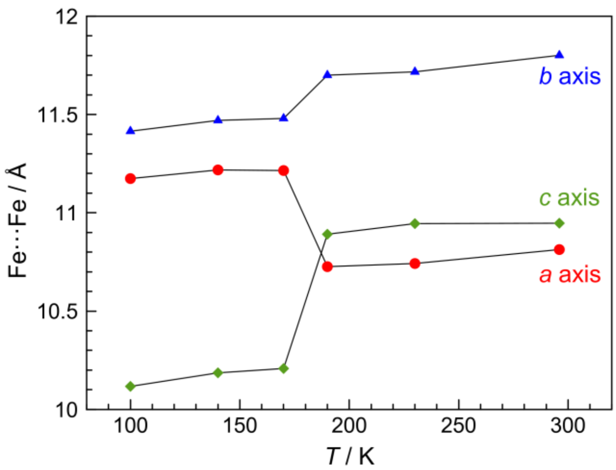

Fig. S15 Temperature dependence of the Fe···Fe distances along the unit cell axes for **1**.

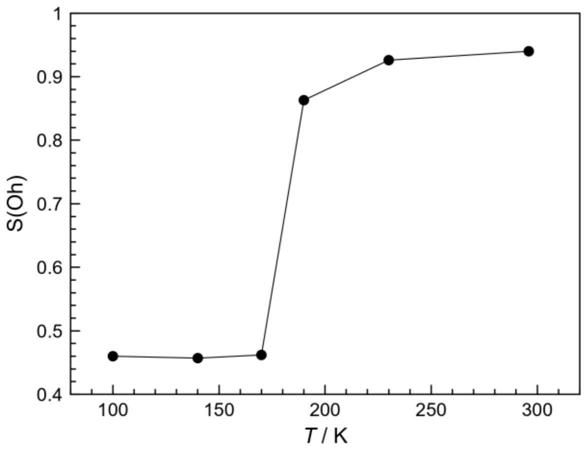

Fig. S16 Temperature dependence of S(Oh) for **1**.

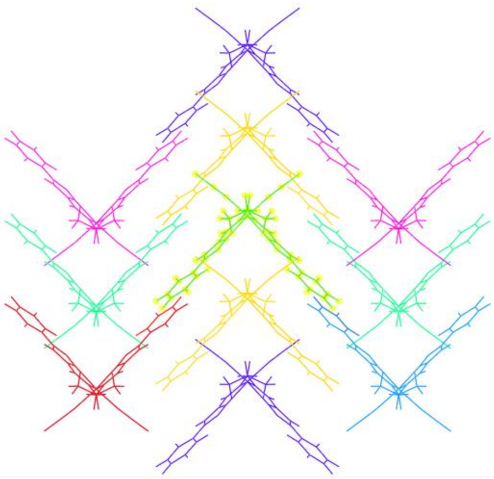

Interaction Energies (kJ/mol)
R is the distance between molecular centroids (mean atomic position) in Å.

Total energies, only reported for two benchmarked energy models, are the sum of the four energy components, scaled appropriately (see the scale factor table below)

	N	Symop	R	Electron Density	E_ele	E_pol	E_dis	E_rep	E_tot
	2	−x, −y, −z	16.87	B3LYP/6-31G(d,p)	3.9	−1.8	−9.6	8.4	−0.4
	4	x+1/2, y+1/2, z	8.00	B3LYP/6-31G(d,p)	−34.5	−23.0	−58.7	45.9	−76.3
	2	x, y, z	10.81	B3LYP/6-31G(d,p)	16.6	−2.1	−11.6	5.1	9.1
	2	−x+1/2, −y+1/2, −z	11.87	B3LYP/6-31G(d,p)	−32.2	−14.6	−61.7	39.8	−74.0
	2	−x, −y, −z	14.43	B3LYP/6-31G(d,p)	9.0	−2.5	−12.3	5.6	0.4
	2	x, y, z	11.80	B3LYP/6-31G(d,p)	−19.1	−8.1	−12.3	8.2	−31.8
	2	−x, −y, −z	11.19	B3LYP/6-31G(d,p)	−63.9	−13.7	−14.9	20.7	−78.0

Scale factors for benchmarked energy models
See Mackenzie et al. IUCrJ (2017)

Energy Model	k_ele	k_pol	k_disp	k_rep
CE-HF ... HF/3-21G electron densities	1.019	0.651	0.901	0.811
CE-B3LYP ... B3LYP/6-31G(d,p) electron densities	1.057	0.740	0.871	0.618

Fig. S17 Molecular structure pairs (left) and the interaction energies (kJ mol^{-1}) calculated using B3LYP-D2/6-31G(d,p) dispersion-corrected DFT model (right) for **1** at 296 K. The total energy ($E_{\_tot}$), electrostatic ($E_{\_ele}$), polarization ($E_{\_pol}$), dispersion ($E_{\_dis}$), and exchange-repulsion ($E_{\_rep}$) components of the energy are listed (kJ mol^{-1}). R indicates the distance between centers of mass of the pair of molecules (Å).

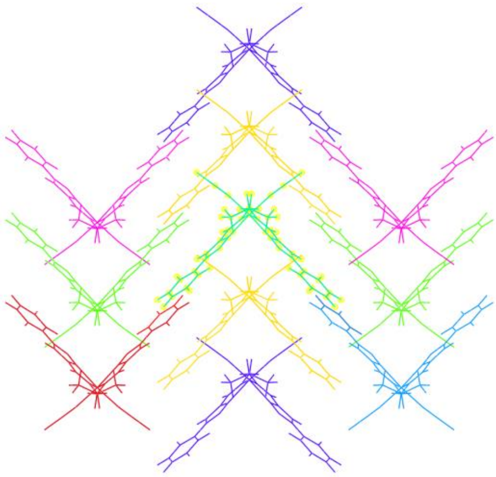

Interaction Energies (kJ/mol)
R is the distance between molecular centroids (mean atomic position) in Å.

Total energies, only reported for two benchmarked energy models, are the sum of the four energy components, scaled appropriately (see the scale factor table below)

	N	Symop	R	Electron Density	E_ele	E_pol	E_dis	E_rep	E_tot
	2	−x, −y, −z	16.83	B3LYP/6-31G(d,p)	3.6	−1.9	−10.1	9.8	−0.3
	4	x+1/2, y+1/2, z	7.95	B3LYP/6-31G(d,p)	−36.1	−23.5	−61.4	50.6	−77.7
	2	−x+1/2, −y+1/2, −z	11.87	B3LYP/6-31G(d,p)	−32.6	−14.6	−63.0	42.4	−73.9
	2	x, y, z	10.74	B3LYP/6-31G(d,p)	16.4	−2.1	−12.1	5.7	8.8
	2	−x, −y, −z	14.41	B3LYP/6-31G(d,p)	8.8	−2.5	−12.8	6.2	0.2
	2	x, y, z	11.72	B3LYP/6-31G(d,p)	−19.1	−8.3	−13.0	9.7	−31.6
	2	−x, −y, −z	11.18	B3LYP/6-31G(d,p)	−65.1	−14.1	−15.4	23.7	−78.1

Scale factors for benchmarked energy models
See Mackenzie et al. IUCrJ (2017)

Energy Model	k_ele	k_pol	k_disp	k_rep
CE-HF ... HF/3-21G electron densities	1.019	0.651	0.901	0.811
CE-B3LYP ... B3LYP/6-31G(d,p) electron densities	1.057	0.740	0.871	0.618

Fig. S18 Molecular structure pairs (left) and the interaction energies (kJ mol^{-1}) calculated using B3LYP-D2/6-31G(d,p) dispersion-corrected DFT model (right) for **1** at 230 K. The total energy ($E_{\_tot}$), electrostatic ($E_{\_ele}$), polarization ($E_{\_pol}$), dispersion ($E_{\_dis}$), and exchange-repulsion ($E_{\_rep}$) components of the energy are listed (kJ mol^{-1}). R indicates the distance between centers of mass of the pair of molecules (Å).

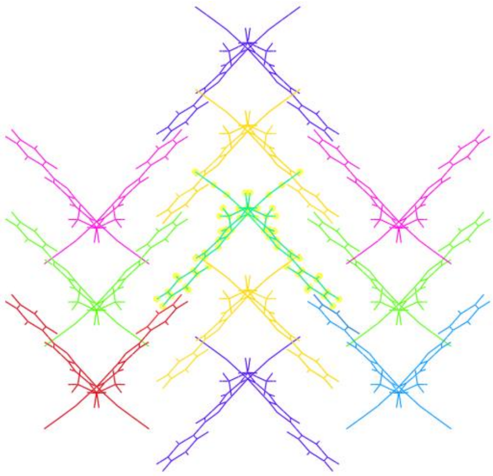

Interaction Energies (kJ/mol)
R is the distance between molecular centroids (mean atomic position) in Å.

Total energies, only reported for two benchmarked energy models, are the sum of the four energy components, scaled appropriately (see the scale factor table below)

	N	Symop	R	Electron Density	E_ele	E_pol	E_dis	E_rep	E_tot
	2	-x, -y, -z	16.83	B3LYP/6-31G(d,p)	3.5	-1.9	-10.2	10.4	-0.2
	4	x+1/2, y+1/2, z	7.94	B3LYP/6-31G(d,p)	-37.2	-23.7	-62.7	53.4	-78.5
	2	-x+1/2, -y+1/2, -z	11.85	B3LYP/6-31G(d,p)	-32.8	-14.6	-63.7	43.7	-73.9
	2	x, y, z	10.73	B3LYP/6-31G(d,p)	16.4	-2.1	-12.0	5.4	8.6
	2	-x, -y, -z	14.37	B3LYP/6-31G(d,p)	8.7	-2.6	-13.1	6.7	0.1
	2	x, y, z	11.70	B3LYP/6-31G(d,p)	-19.0	-8.3	-13.2	10.2	-31.5
	2	-x, -y, -z	11.12	B3LYP/6-31G(d,p)	-65.5	-14.2	-15.8	24.8	-78.2

Scale factors for benchmarked energy models
See Mackenzie et al. IUCrJ (2017)

Energy Model	k_ele	k_pol	k_disp	k_rep
CE-HF ... HF/3-21G electron densities	1.019	0.651	0.901	0.811
CE-B3LYP ... B3LYP/6-31G(d,p) electron densities	1.057	0.740	0.871	0.618

Fig. S19 Molecular structure pairs (left) and the interaction energies (kJ mol^{-1}) calculated using B3LYP-D2/6-31G(d,p) dispersion-corrected DFT model (right) for **1** at 190 K. The total energy ($E_{\_tot}$), electrostatic ($E_{\_ele}$), polarization ($E_{\_pol}$), dispersion ($E_{\_dis}$), and exchange-repulsion ($E_{\_rep}$) components of the energy are listed (kJ mol^{-1}). R indicates the distance between centers of mass of the pair of molecules (Å).

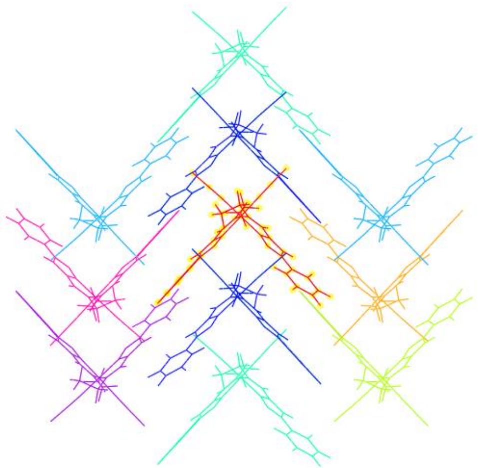

Interaction Energies (kJ/mol)
R is the distance between molecular centroids (mean atomic position) in Å.

Total energies, only reported for two benchmarked energy models, are the sum of the four energy components, scaled appropriately (see the scale factor table below)

	N	Symop	R	Electron Density	E_ele	E_pol	E_dis	E_rep	E_tot
	2	x, y, z	11.21	B3LYP/6-31G(d,p)	15.3	-1.6	-11.5	6.8	9.2
	1	-x, -y, -z	11.23	B3LYP/6-31G(d,p)	-35.1	-16.1	-77.2	60.3	-79.1
	2	x, -y+1/2, z+1/2	13.66	B3LYP/6-31G(d,p)	10.0	-3.7	-16.0	9.9	-0.0
	2	-x, y+1/2, -z+1/2	7.93	B3LYP/6-31G(d,p)	-35.9	-24.8	-67.5	53.4	-82.1
	2	x, y, z	11.48	B3LYP/6-31G(d,p)	-22.0	-9.9	-15.4	14.9	-34.8
	2	x, -y+1/2, z+1/2	10.49	B3LYP/6-31G(d,p)	-72.1	-17.2	-17.4	25.4	-88.4
	2	-x, y+1/2, -z+1/2	8.12	B3LYP/6-31G(d,p)	-37.6	-24.0	-60.3	52.7	-77.5
	2	x, -y+1/2, z+1/2	16.71	B3LYP/6-31G(d,p)	4.1	-1.7	-9.2	7.8	-0.2
	1	-x, -y, -z	11.59	B3LYP/6-31G(d,p)	-37.2	-16.3	-70.5	55.4	-78.5

Scale factors for benchmarked energy models
See Mackenzie et al. IUCrJ (2017)

Energy Model	k_ele	k_pol	k_disp	k_rep
CE-HF ... HF/3-21G electron densities	1.019	0.651	0.901	0.811
CE-B3LYP ... B3LYP/6-31G(d,p) electron densities	1.057	0.740	0.871	0.618

Fig. S20 Molecular structure pairs (left) and the interaction energies (kJ mol^{-1}) calculated using B3LYP-D2/6-31G(d,p) dispersion-corrected DFT model (right) for **1** at 170 K. The total energy ($E_{\_tot}$), electrostatic ($E_{\_ele}$), polarization ($E_{\_pol}$), dispersion ($E_{\_dis}$), and exchange-repulsion ($E_{\_rep}$) components of the energy are listed (kJ mol^{-1}). R indicates the distance between centers of mass of the pair of molecules (Å).

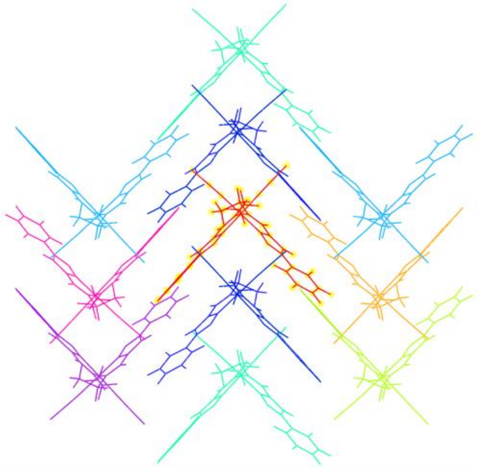

Interaction Energies (kJ/mol)
R is the distance between molecular centroids (mean atomic position) in Å.

Total energies, only reported for two benchmarked energy models, are the sum of the four energy components, scaled appropriately (see the scale factor table below)

	N	Symop	R	Electron Density	E_ele	E_pol	E_dis	E_rep	E_tot
	2	x, y, z	11.22	B3LYP/6-31G(d,p)	15.1	-1.6	-11.6	7.0	9.0
	1	-x, -y, -z	11.22	B3LYP/6-31G(d,p)	-35.3	-16.0	-78.4	62.8	-78.7
	2	x, -y+1/2, z+1/2	13.64	B3LYP/6-31G(d,p)	9.9	-3.7	-16.1	10.1	-0.1
	2	-x, y+1/2, -z+1/2	7.93	B3LYP/6-31G(d,p)	-36.0	-24.7	-68.6	54.7	-82.3
	2	x, y, z	11.47	B3LYP/6-31G(d,p)	-21.8	-9.9	-15.6	15.7	-34.3
	2	x, -y+1/2, z+1/2	10.46	B3LYP/6-31G(d,p)	-72.3	-17.3	-17.6	26.3	-88.3
	2	-x, y+1/2, -z+1/2	8.12	B3LYP/6-31G(d,p)	-37.9	-24.0	-60.6	53.3	-77.7
	2	x, -y+1/2, z+1/2	16.70	B3LYP/6-31G(d,p)	4.0	-1.7	-9.3	8.0	-0.2
	1	-x, -y, -z	11.58	B3LYP/6-31G(d,p)	-37.4	-16.3	-71.5	57.5	-78.4

Scale factors for benchmarked energy models
See Mackenzie et al. IUCrJ (2017)

Energy Model	k_ele	k_pol	k_disp	k_rep
CE-HF ... HF/3-21G electron densities	1.019	0.651	0.901	0.811
CE-B3LYP ... B3LYP/6-31G(d,p) electron densities	1.057	0.740	0.871	0.618

Fig. S21 Molecular structure pairs (left) and the interaction energies (kJ mol^{-1}) calculated using B3LYP-D2/6-31G(d,p) dispersion-corrected DFT model (right) for **1** at 140 K. The total energy ($E_{\_tot}$), electrostatic ($E_{\_ele}$), polarization ($E_{\_pol}$), dispersion ($E_{\_dis}$), and exchange-repulsion ($E_{\_rep}$) components of the energy are listed (kJ mol^{-1}). R indicates the distance between centers of mass of the pair of molecules (Å).

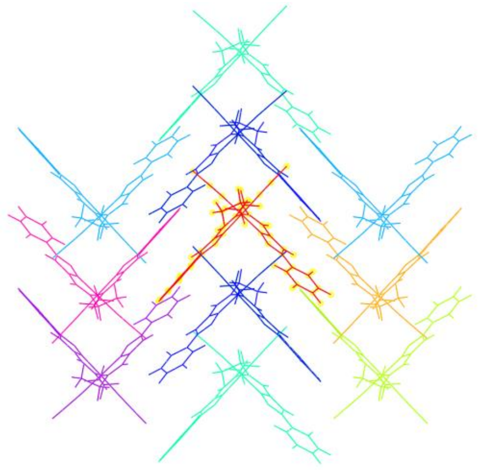

Interaction Energies (kJ/mol)
R is the distance between molecular centroids (mean atomic position) in Å.

Total energies, only reported for two benchmarked energy models, are the sum of the four energy components, scaled appropriately (see the scale factor table below)

	N	Symop	R	Electron Density	E_ele	E_pol	E_dis	E_rep	E_tot
	2	x, y, z	11.17	B3LYP/6-31G(d,p)	14.9	-1.6	-12.0	7.5	8.9
	1	-x, -y, -z	11.15	B3LYP/6-31G(d,p)	-36.5	-16.4	-81.6	68.4	-79.5
	2	x, -y+1/2, z+1/2	13.56	B3LYP/6-31G(d,p)	9.8	-3.8	-16.8	11.0	-0.3
	2	-x, y+1/2, -z+1/2	7.89	B3LYP/6-31G(d,p)	-37.0	-25.1	-71.1	59.0	-83.1
	2	x, y, z	11.41	B3LYP/6-31G(d,p)	-22.2	-10.1	-16.2	17.2	-34.5
	2	x, -y+1/2, z+1/2	10.39	B3LYP/6-31G(d,p)	-73.7	-17.8	-18.3	29.0	-89.2
	2	-x, y+1/2, -z+1/2	8.09	B3LYP/6-31G(d,p)	-38.9	-24.4	-62.6	57.3	-78.3
	2	x, -y+1/2, z+1/2	16.62	B3LYP/6-31G(d,p)	3.9	-1.7	-9.6	8.6	-0.3
	1	-x, -y, -z	11.51	B3LYP/6-31G(d,p)	-38.6	-16.7	-74.4	62.8	-79.2

Scale factors for benchmarked energy models
See Mackenzie et al. IUCrJ (2017)

Energy Model	k_ele	k_pol	k_disp	k_rep
CE-HF ... HF/3-21G electron densities	1.019	0.651	0.901	0.811
CE-B3LYP ... B3LYP/6-31G(d,p) electron densities	1.057	0.740	0.871	0.618

Fig. S22 Molecular structure pairs (left) and the interaction energies (kJ mol^{-1}) calculated using B3LYP-D2/6-31G(d,p) dispersion-corrected DFT model (right) for **1** at 100 K. The total energy ($E_{\_tot}$), electrostatic ($E_{\_ele}$), polarization ($E_{\_pol}$), dispersion ($E_{\_dis}$), and exchange-repulsion ($E_{\_rep}$) components of the energy are listed (kJ mol^{-1}). R indicates the distance between centers of mass of the pair of molecules (Å).

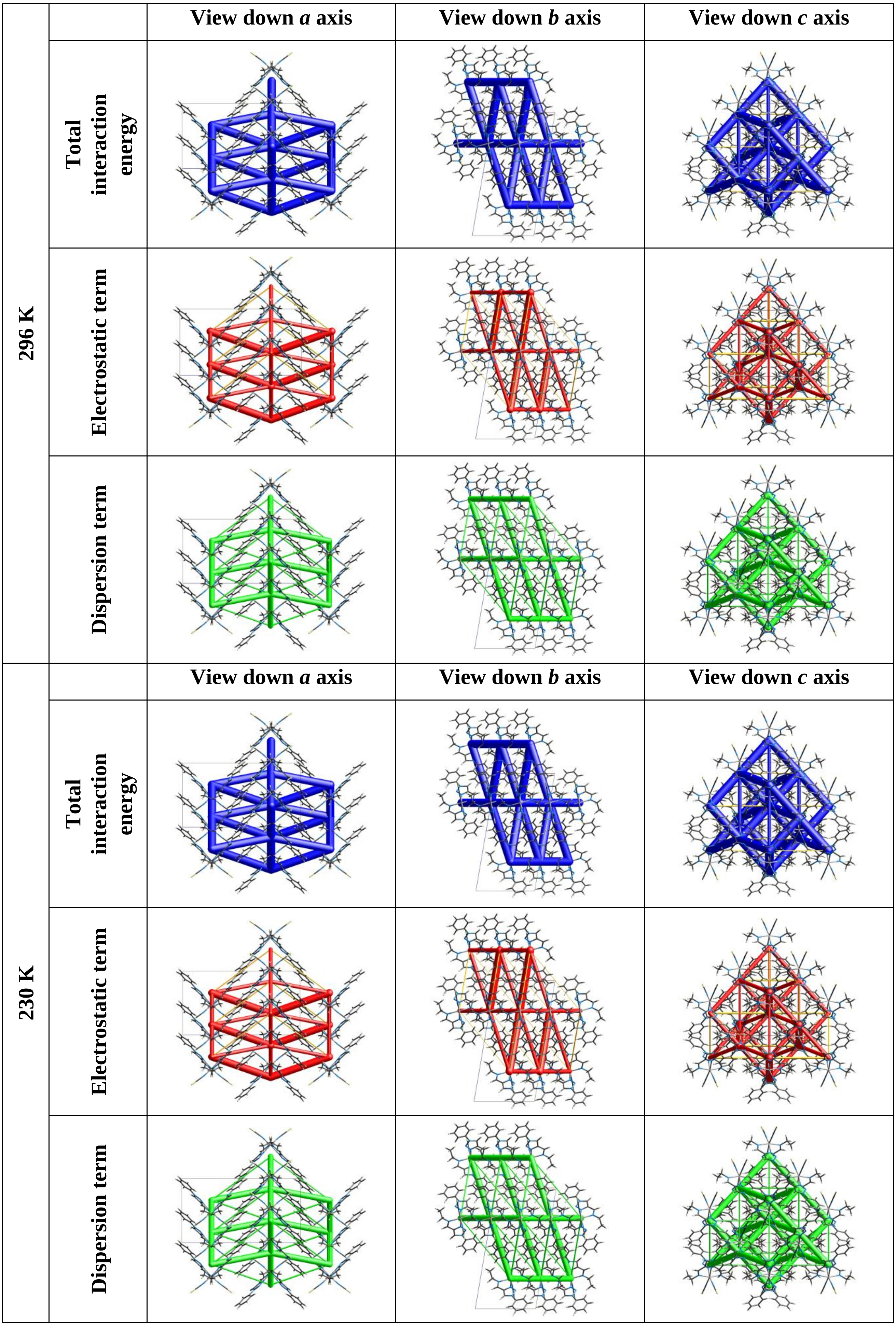

Fig. S23 Energy frameworks of **1** at 296 and 230 K viewed along three different crystallographic directions.

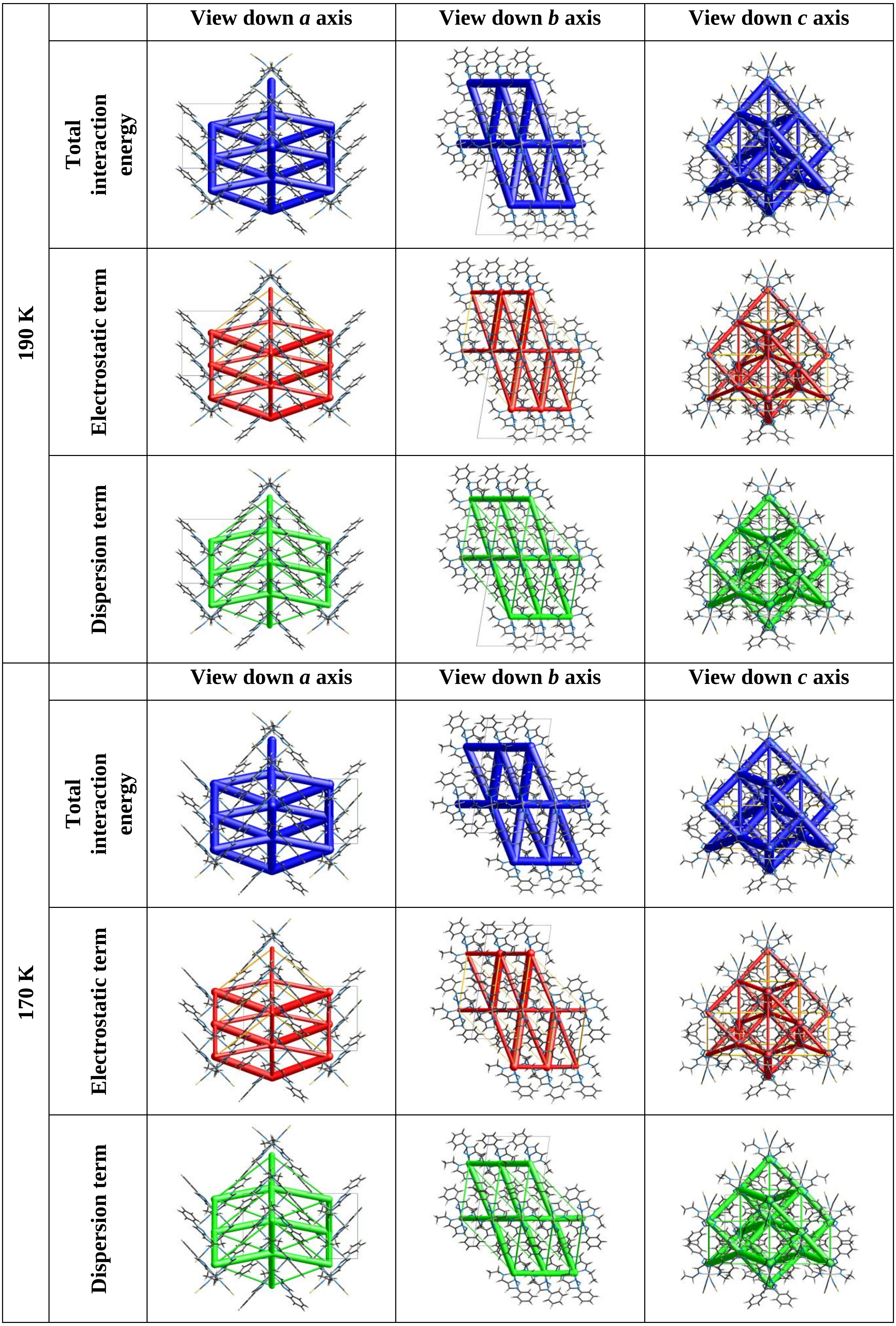

Fig. S24 Energy frameworks of **1** at 190 and 170 K viewed along three different crystallographic directions.

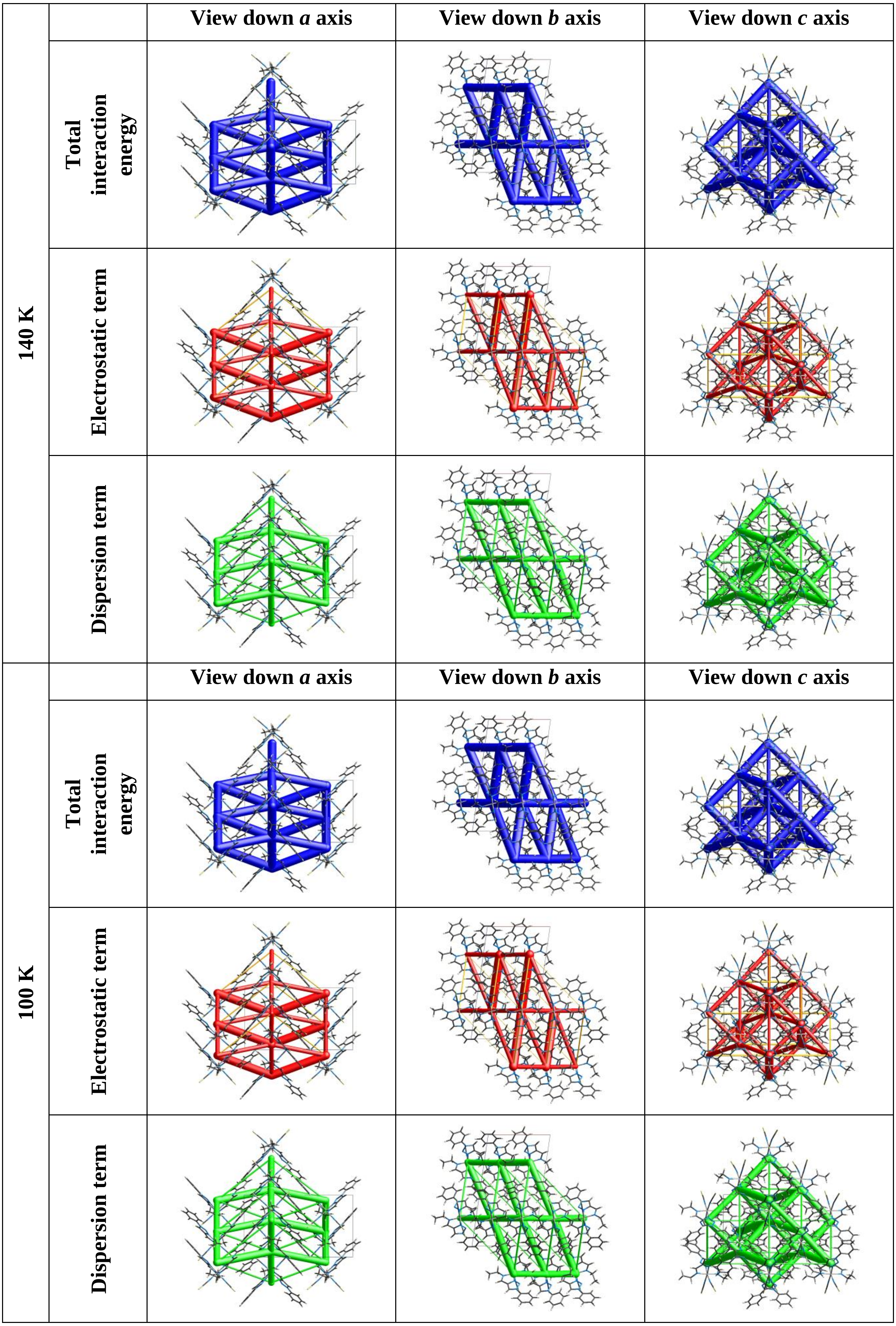

Fig. S25 Energy frameworks of **1** at 140 and 100 K viewed along three different crystallographic directions.

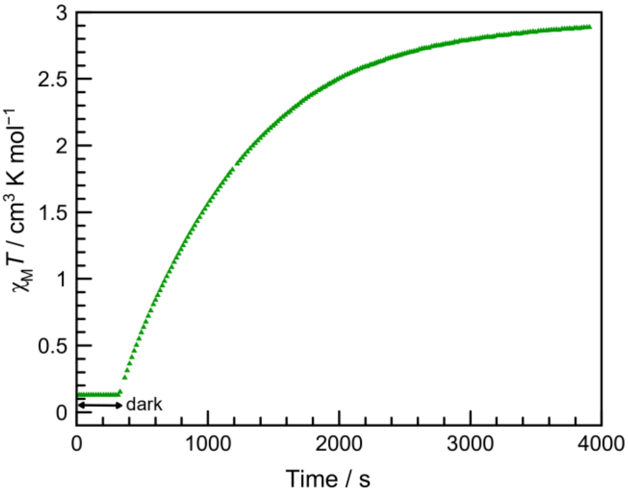

Fig. S26 Time dependence of the $\chi_M T$ product of **1** under 532 nm light irradiation at 10 K.

References

S1 P. Guionneau, M. Marchivie, G. Bravic, J.-F. Létard and D. Chasseau, *Top. Curr. Chem.* 2004, **234**, 97–128.

S2 R. Ketkaew, Y. Tantirungrotechai, P. Harding, G. Chastanet, P. Guionneau, M. Marchivie and D. J. Harding, *Dalton Trans.*, 2021, **50**, 1086–1096.

S3 M. Marchivie, P. Guionneau, J.-F. Létard and D. Chasseau, *Acta Crystallogr., Sect. B: Struct. Sci.*, 2005, **61**, 25–28.

S4 O. V. Dolomanov, L. J. Bourhis, R. J. Gildea, J. A. K. Howard and H. Puschmann, *J. Appl. Crystallogr.*, 2009, **42**, 339–341.

S5 M. Llunell, D. Casanova, J. Cirera, P. Alemany and S. Alvarez, *SHAPE2.1. Program for Calculating Continuous Shape Measures of Polyhedral Structures*, Universitat de Barcelona, Barcelona, 2013.

Legends to the Supplementary Movies

Movie S1 Cold-stage (liquid N_2) microscopy of single crystals of **1** upon first cooling (75 °C min^{-1}) from 20 °C to –180 °C, showing the thermosalient effect.

Movie S2 Cold-stage (liquid N_2) microscopy of single crystals of **1** upon first heating (75 °C min^{-1}) from –180 °C to 20 °C, showing no thermosalience.

Movie S3 Cold-stage (liquid N_2) microscopy of single crystals of **1** upon second cooling (75 °C min^{-1}) from 20 °C to –180 °C, showing no thermosalience.

Movie S4 Cold-stage (liquid N_2) microscopy of single crystals of **1** upon second heating (75 °C min^{-1}) from –180 °C to 20 °C, showing no thermosalience.

Movie S5 Cold-stage (liquid N_2) microscopy of single crystals of **1** upon third cooling (75 °C min^{-1}) from 20 °C to –180 °C, showing no thermosalience.

Movie S6 Cold-stage (liquid N_2) microscopy of single crystals of **1** upon third heating (75 °C min^{-1}) from –180 °C to 20 °C, showing no thermosalience.

Movie S7-1 Cold-stage (liquid N_2) microscopy of single crystals of **1** upon first cooling (75 °C min^{-1}) from 20 °C to –90 °C, showing no thermosalience.

Movie S7-2 Cold-stage (liquid N_2) microscopy of single crystals of **1** upon first cooling (75 °C min^{-1}) from –90 °C to –105 °C, showing the thermosalient effect.

Movie S7-3 Cold-stage (liquid N_2) microscopy of single crystals of **1** upon first cooling (75 °C min^{-1}) from –105 °C to –180 °C, showing no thermosalience.

Movie S8-1 Cold-stage (liquid N_2) microscopy of single crystals of **1** upon first cooling (75 °C min^{-1}) from –90 °C to –91 °C and subsequent holding the temperature, showing no thermosalience.

Movie S8-2 Cold-stage (liquid N_2) microscopy of single crystals of **1** upon first cooling (75 °C min^{-1}) from –91 °C to –92 °C and subsequent holding the temperature, showing no thermosalience.

Movie S8-3 Cold-stage (liquid N_2) microscopy of single crystals of **1** upon first cooling (75 °C min^{-1}) from –92 °C to –93 °C and subsequent holding the temperature, showing no thermosalience.

Movie S8-4 Cold-stage (liquid N_2) microscopy of single crystals of **1** upon first cooling (75 °C min^{-1}) from –93 °C to –94 °C and subsequent holding the temperature, showing no thermosalience.

Movie S8-5 Cold-stage (liquid N_2) microscopy of single crystals of **1** upon first cooling (75 °C min^{-1}) from –94 °C to –95 °C and subsequent holding the temperature, showing no thermosalience.

Movie S8-6 Cold-stage (liquid N_2) microscopy of single crystals of **1** upon first cooling (75 °C min^{-1}) from –95 °C to –96 °C and subsequent holding the temperature, showing the thermosalient effect.

Movie S8-7 Cold-stage (liquid N_2) microscopy of single crystals of **1** upon first cooling (75 °C min^{-1}) from –96 °C to –97 °C and subsequent holding the temperature, showing the thermosalient effect.

Movie S8-8 Cold-stage (liquid N_2) microscopy of single crystals of **1** upon first cooling (75 °C min^{-1}) from –97 °C to –98 °C and subsequent holding the temperature, showing the thermosalient effect.

Movie S8-9 Cold-stage (liquid N_2) microscopy of single crystals of **1** upon first cooling (75 °C min^{-1}) from –98 °C to –99 °C and subsequent holding the temperature, showing no thermosalience.

Movie S8-10 Cold-stage (liquid N_2) microscopy of single crystals of **1** upon first cooling (75 °C min^{-1}) from –99 °C to –100 °C and subsequent holding the temperature, showing no thermosalience.

Movie S8-11 Cold-stage (liquid N_2) microscopy of single crystals of **1** upon first cooling (75 °C min^{-1}) from –100 °C to –101 °C and subsequent holding the temperature, showing no thermosalience.

Movie S8-12 Cold-stage (liquid N_2) microscopy of single crystals of **1** upon first cooling (75 °C min^{-1}) from –101 °C to –102 °C and subsequent holding the temperature, showing no thermosalience.

Movie S8-13 Cold-stage (liquid N_2) microscopy of single crystals of **1** upon first cooling (75 °C min^{-1}) from –102 °C to –103 °C and subsequent holding the temperature, showing no thermosalience.

Movie S8-14 Cold-stage (liquid N_2) microscopy of single crystals of **1** upon first cooling (75 °C min^{-1}) from –103 °C to –104 °C and subsequent holding the temperature, showing no thermosalience.

Movie S8-15 Cold-stage (liquid N_2) microscopy of single crystals of **1** upon first cooling (75 °C min^{-1}) from –104 °C to –105 °C and subsequent holding the temperature, showing no thermosalience.